LA-UR-14-27991
Approved for public release; distribution is unlimited.

Title: Electron and ion heating by whistler turbulence: Three-dimensional particle-in-cell simulations

Author(s): Hughes, R. Scott
Gary, Stephen Peter
Wang, Joseph

Intended for: Geophysical Research Letters

Issued: 2014-10-14

Electron and ion heating by whistler turbulence: Three-dimensional particle-in-cell simulations

R. Scott Hughes[1], S. Peter Gary[2], and Joseph Wang[3]

10 October 2014

Abstract

Three-dimensional particle-in-cell simulations of decaying whistler turbulence are carried out on a collisionless, homogeneous, magnetized, electron-ion plasma model. The simulations use an initial ensemble of relatively long wavelength whistler modes with a broad range of initial propagation directions with an initial electron beta $\beta_e = 0.05$. The computations follow the temporal evolution of the fluctuations as they cascade into broadband turbulent spectra at shorter wavelengths. Three simulations correspond to successively larger simulation boxes and successively larger wavelengths of the initial fluctuations. The computations confirm previous results showing electron heating is preferentially parallel to the background magnetic field $\mathbf{B_o}$, and ion heating is preferentially perpendicular to $\mathbf{B_o}$. The new results here are that larger simulation boxes and longer initial whistler wavelengths yield weaker electron heating, stronger ion heating, and weaker overall dissipation.

Introduction

[1] University of Southern California, Los Angeles, CA
[2] Space Science Institute, Boulder, CO
[3] University of Southern California, Los Angeles, CA

Solar wind protons, as they flow away from the Sun in a slowly decreasing magnetic field, should become strongly anisotropic in the sense of $T_\perp << T_{||}$ due to conservation of their magnetic moments (Here $\perp$ and || denote directions relative to the background magnetic field $\mathbf{B_0}$.). But proton velocity distributions near 1 AU are typically observed to be relatively isotropic, indicating that one or more plasma processes are acting to scatter such particles from parallel toward perpendicular velocities [*Hellinger et al.,* 2011; 2013]; an exhaustive list of possible such processes is presented in Section 2 of *Cranmer* [2014]. Two of the more popular of these processes are nonresonant ion scattering by low-frequency, long-wavelength magnetohydrodynamic (MHD) fluctuations including a nonlinear mechanism called "stochastic heating" (*Chandran et al.,* 2010; *Xia et al.,* 2013 and citations therein), and quasilinear ion cyclotron resonant scattering by Alfven-cyclotron fluctuations somewhat below the proton cyclotron frequency and $k_{||}c/\omega_p \leq 1$ (*Hollweg and Isenberg,* 2002; *Gary and Saito,* 2003; *Cranmer,* 2014, and citations therein) where ω_p denotes the proton plasma frequency. Recently *Saito and Nariyuki* [2014] used two-dimensional particle-in-cell (PIC) simulations to show that decaying whistler turbulence can transfer energy to ions preferentially in directions perpendicular to $\mathbf{B_0}$, thereby arguing that whistler turbulence can also be a contributing mechanism to ion heating in the solar wind. This manuscript describes three-dimensional (3D) PIC simulations which extend the work of *Saito and Nariyuki* [2014] and in particular demonstrate that the perpendicular ion heating by whistler turbulence becomes stronger as successively longer wavelength fluctuations are considered.

Turbulence may be defined as an ensemble of enhanced, incoherent, broadband fluctuations. Such phenomena in magnetized, collisionless, ionized media may be empirically divided into long-wavelength plasma turbulence, with magnetic fluctuation spectra following a power-law wavenumber dependence $\sim k^{5/3}$ (the "inertial range"), and short-wavelength plasma turbulence, with much steeper fluctuation spectra $\sim k^{-\alpha}$ where $\alpha > 2$ (the "kinetic range"). Solar wind observations of plasma turbulence spectra conclude that the spectral break between the two ranges scale approximately as $k\lambda_p \sim 1$, where λ_p is the proton inertial length [*Bourouaine et al.,* 2012], or as $k\rho_p \sim 1$, where ρ_p is the thermal proton gyroradius, or as a combination of these two scales and the fluctuation amplitude at those scales [*Markovskii et al.,* 2008]. The thermal proton beta β_p of the solar wind is typically of order unity, so it has been difficult to resolve the wavenumber scaling of this spectral break in that medium. However, there is general agreement that the spectral break marks the boundary between the long-wavelength regime in which fluid theories such as magnetohydrodynamics (MHD) provide an adequate description of the turbulence and the short-wavelength regime which requires a velocity-space (i.e., "kinetic") description of the turbulence.

Two competing hypotheses have been proposed to describe the character of short-wavelength turbulence in the solar wind. One scenario is that this turbulence consists of kinetic Alfven waves which propagate in directions quasi-perpendicular to the background magnetic field $\mathbf{B}_o$ and at real frequencies $\omega_r < \Omega_p$ where the latter symbol represents the proton cyclotron frequency. Both solar wind observations [*Leamon et al.,* 1998; *Bale et al.,* 2005; *Sahraoui et al.,* 2009, 2010; *He et al.,* 2012; *Salem et al.,* 2012;

67 *Chen et al.,* 2013, *Kiyani et al.,* 2013] and gyrokinetic simulations [*Howes et al.,* 2008a,
68 2008b, 2011; *Matthaeus et al.,* 2008; *TenBarge et al.,* 2013] of turbulence have been
69 interpreted as consisting of kinetic Alfven waves. While it is likely that the turbulence
70 measured immediately above the inertial range spectral break does consist of kinetic
71 Alfven waves, there is debate as to whether or not such modes can cascade fluctuation
72 energy down to the very short wavelengths of electron inertial ($k\lambda_e \sim 1$) or thermal
73 electron gyroradius ($k\rho_e \sim 1$) scales [*Podesta et al.,* 2010; *Smith et al.,* 2012; *Sahraoui et*
74 *al.,* 2013]. A second hypothesis is that magnetosonic-whistler fluctuations between the
75 proton cyclotron and electron cyclotron frequencies also contribute to such turbulence.
76 Solar wind measurements provide evidence for magnetosonic-whistler and Bernstein
77 mode contributions to short-wavelength turbulence [*Narita et al.,* 2011; *Perschke et al.,*
78 2013, 2014]. Particle-in-cell simulations have been used to address the forward cascades
79 of magnetosonic turbulence [*Svidzinski et al.,* 2009] and whistler turbulence [*Saito et al.,*
80 2008, 2010; *Saito and Gary,* 2012; *Chang et al.,* 2011, 2013, 2014; *Gary et al.,* 2008,
81 2012].
82
83 Whistler PIC simulations show in particular that forward cascades give rise to
84 turbulence with a preference for quasi-perpendicular propagation relative to $\mathbf{B}_o$. This
85 $k_\perp >> k_{||}$ wavevector anisotropy implies that whistler modes at $kc/\omega_e < 1$ should have
86 substantial parallel electric field components, so that the Landau resonance is the primary
87 means of wave dissipation on the magnetized electrons and the consequent heating
88 should yield $T_{||e} > T_{\perp e}$ as the body of PIC whistler turbulence simulations have
89 demonstrated. The same wavenumber anisotropy further implies that the electrostatic

90 component of the fluctuating electric fields should provide the dominant contribution to
91 $\delta \boldsymbol{E}$ [e.g., Fig. 6.8 of *Gary* (1993)], so that the primary heating on the relatively
92 unmagnetized ions should yield $T_{||i}<T_{\perp i}$, as has been argued by *Saito and Nariyuki* [2014]
93 and as their simulations have demonstrated.
94
95 Whistler turbulence PIC simulations have, except for *Saito and Nariyuki* [2014],
96 addressed only electron heating, but *Howes* [2010] used a cascade model to conclude that
97 kinetic Alfven turbulence should preferentially heat ions at $\beta_i > 2.5$, and heat electrons
98 more strongly at smaller values of the ion beta [*TenBarge and Howes,* 2013]. This
99 manuscript reports PIC simulations of decaying whistler turbulence with analyses of how
100 the field fluctuation energy is dissipated on both the electrons and the ions. Consistent
101 with the results of *Saito and Nariyuki* (2014), the ions are heated with $T_{\perp i} > T_{||i}$, although
102 more weakly than the electrons with $T_{||e} >> T_{\perp e}$. Here we quantitatively compare
103 electron and ion heating for several different simulation box sizes, demonstrating that the
104 relative ion heating increases as larger simulation systems admit longer wavelengths
105 which allow the ion Landau resonance to become stronger.
106
107 **Simulations**
108 The simulations described here are carried out using the three-dimensional (3D)
109 electromagnetic particle-in-cell code 3D-EMPIC which is a further development of the
110 code described by *Wang et al.* [1995]. Here "three-dimensional" means that the
111 simulations includes variations in three spatial dimensions, as well as calculating the full

112 3D velocity-space response of each ion and electron superparticle. With this code,
113 superparticles are advanced using a standard relativistic particle algorithm, currents are
114 computed using a rigorous charge conservation scheme [*Villasenor and Buneman,* 1992],
115 and the self-consistent electromagnetic fields are solved using a local finite difference
116 time domain solution to the full Maxwell's equations.
117
118 Our simulations model a collisionless, homogeneous, magnetized electron-ion
119 plasma. The problem addressed is the same as that studied by *Chang et al.* [2011, 2013,
120 2014] and *Gary et al.* [2012]; an ensemble of relatively long-wavelength, approximately
121 isotropic whistler fluctuations are imposed at $t=0$, and the simulations follow the
122 subsequent temporal evolution of the fluctuating fields and the particles. The whistler
123 modes undergo a forward cascade to a broadband turbulent spectrum at shorter
124 wavelengths, while at the same time the plasma is heated. One important difference
125 between the *Chang et al.* simulations and the computations described here is the initial
126 conditions on the ions. The earlier simulations were concerned only with the interactions
127 between the fluctuations and the electrons, so that the initial ion velocity distributions
128 were taken to be Maxwellian. Here we wish to compare electron and ion heating, so that
129 we have taken care to initialize both the electron and ion velocity distributions to reflect
130 both species responses to the initial spectrum of whistler waves.
131
132 Our earlier PIC simulations of whistler turbulence evaluated the transfer of field
133 fluctuation energy only to the electrons. Here, following *Saito and Nariyuki* [2014], we
134 examine the ion heating as well. To facilitate the comparison of dissipation on both

135 species, we use $m_i/m_e = 400$; other physical initial conditions include isotropic
136 Maxwellian velocity distributions for both species with $T_e = T_i$, $\beta_j \equiv 8\pi\, n_j\, k_B\, T_j/B_o^2$ where
137 $j = e$ for electrons and $j = i$ for ions with $\beta_e = \beta_i = 0.05$. The electron thermal speed is
138 denoted by $v_e = (k_B\, T_e/m_e)^{1/2}$ and at $t = 0$ $v_e^2/c^2 = 0.01$. The initial dimensionless
139 fluctuating magnetic field energy density is defined as $\varepsilon_o \equiv \Sigma_k\, |\delta \boldsymbol{B}(\boldsymbol{k})|^2\, /B_o^2$, and we
140 choose $\varepsilon_o = 0.10$.
141
142 The computational parameters are as follows: the grid spacing is $\Delta = 0.10\ c/\omega_e$
143 where ω_e is the electron plasma frequency, the time step is $\delta t\ \omega_e = 0.05$, and the number
144 of superparticles per cell is 64 with 32 electrons and 32 ions. Our simulations are carried
145 out on a cube of size $L_x=L_y=L_z=L$. We have executed three computations at $L\omega_e/c$
146 =25.6, 51.2, and 102.4, corresponding respectively to 256^3, 512^3, and 1024^3 simulation
147 cells and fundamental wavenumbers of, respectively, $k_{xo}c/\omega_e = 0.2454$, 0.1227, and
148 0.0614. The initial spectra then correspond to arrays of 150 whistler modes that are
149 relatively isotropic (The $k_\perp = 0$ whistler modes have well-defined dispersion properties,
150 but there are no whistler fluctuations at $k_\parallel = 0$.), distributed as described in *Gary et al.*
151 [2012].
152
153 Here our concern is the relative heating of electrons versus ions, and that
154 comparison is shown in Figure 1. The first four panels of this figure confirm earlier
155 simulation results that whistler turbulence preferentially heats electrons in directions
156 parallel to $\mathbf{B_o}$ [*Saito et al.,* 2008; *Gary et al.,* 2012; *Chang et al.,* 2013], and preferentially
157 heats ions in directions perpendicular to the background magnetic field [*Saito and*

Nariyuki, 2014]. Comparison of panels (a) and (d) of Figure 1 shows a new result, that the longer wavelength whistler turbulence associated with larger simulation boxes provides less dissipative energy to the electrons but more such energy to the ions. Furthermore, Figure 1e shows that, for these three simulations, the total dissipation of the magnetic field fluctuations decreases as the simulation box size (and the overall wavelengths of the turbulence) increases. This is consistent with Fig. 7(b) of *Saito et al.* [2008] which shows linear theory damping of whistlers at quasi-perpendicular propagation decreasing as wavelengths increase. The linear theory damping is due to the Landau wave-particle resonance, and we infer that the same mechanism is heating the electrons and the ions in our simulations although nonlinear processes certainly contribute to the heating as the fluctuation amplitudes increase [e.g., *Chang et al.,* 2014].

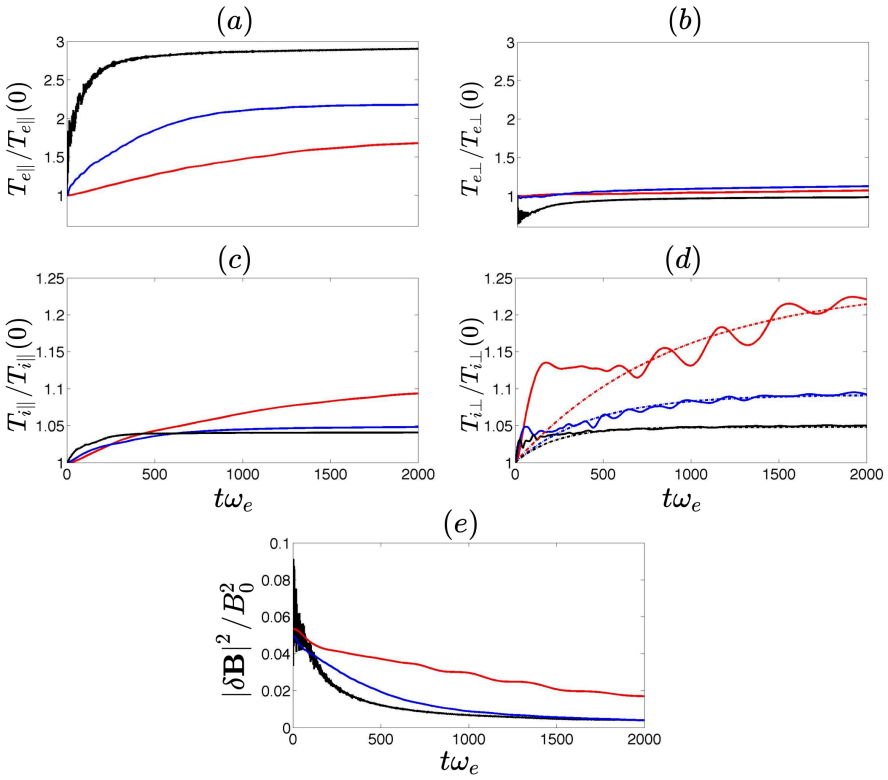

Figure 1. Simulation histories of the (a) parallel electron, (b) perpendicular electron, (c) parallel ion and (d) perpendicular ion temperatures as functions of time from the runs with 256^3 cells (black lines), 512^3 cells (blue lines), and 1024^3 cells (red lines). Panel (e) shows the simulation histories of the total magnetic field fluctuation energy for the same three cases. The dashed lines represent fits to the equation $T_{\perp i}/ T_{\perp i}(0) = 1 + a[1-exp(-bt)]$ with a=0.048 and b=0.0043 for the 256^3 run, a=0.092 and b=0.0023 for the 512^3 run, and a=0.240 and b=0.0011 for the 1024^3 run.

Figure 2 illustrates the reduced electron parallel velocity distributions and ion perpendicular velocity distributions at selected times for each of the three simulations. The figures show that the transfer of fluctuation energy to both the electrons and ions is indeed a heating process, because the late-time velocity distributions of both species for the most part retain their thermal, Maxwellian-like character even as they gain energy. The primary late-time departures from Maxwellian forms are on the electron parallel velocity distributions in the presence of enhanced high-speed "tails" for the runs at 256^3 and 512^3. This feature is a typical electron response to obliquely propagating whistlers at $\beta_e << 1$, and is discussed in detail in *Chang et al.* [2013].

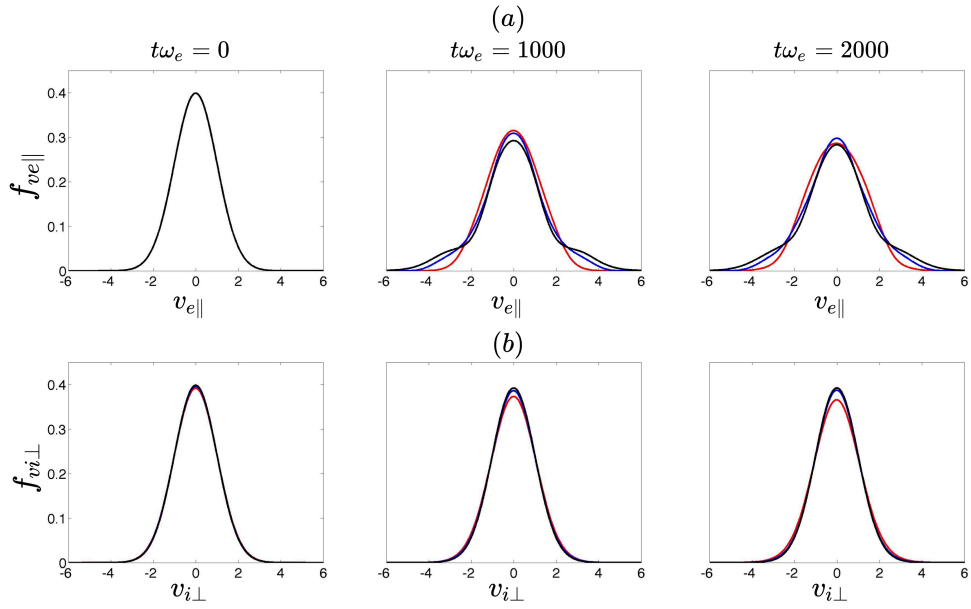

Figure 2. Reduced species velocity distributions from the three simulations at $\omega_e t$= 0, 1000, and 2000 as labeled for (upper row) electron parallel velocities and (lower row) ion perpendicular component velocities. Results are from the runs with 256^3 cells (black lines), 512^3 cells (blue lines), and 1024^3 cells (red lines).

Conclusions

We have used fully three-dimensional, fully kinetic particle-in-cell simulations to examine how decaying whistler turbulence in a low-β collisionless plasma dissipates energy on both electrons and protons. Our computations confirm previous results showing electron heating is preferentially parallel to the background magnetic field $\mathbf{B_o}$, and ion heating is preferentially perpendicular to $\mathbf{B_o}$.

202 The new results here are that larger simulation boxes and longer initial whistler
203 wavelengths yield weaker electron heating, stronger ion heating, and weaker overall
204 dissipation.

205 The interpretation of anisotropic electron and ion heating by whistler turbulence
206 in the weak fluctuation limit is direct; the $k_\perp >> k_{||}$ wavevector anisotropy which usually
207 results from the forward whistler cascade implies the Landau resonance dominates the
208 wave-particle interactions at $kc/\omega_e < 1$ and yields preferential parallel heating on the
209 electrons and perpendicular heating on the ions. The relative heating of the two plasma
210 species as a function of the simulation box size requires a more involved interpretation,
211 as follows. In the computations described above, a larger simulation box corresponds to
212 larger values of the initial whistler wavelengths, so that the initial $k_{||}$ and $k_\perp$ are both
213 smaller. In the limits of $kc/\omega_i >> 1$ and $kc/\omega_e << 1$, linear dispersion theory predicts that
214 the whistler frequency is $\omega_r/\Omega_e \cong k k_{||} c^2/\omega_e^2$. Heating of the ions, which are essentially
215 unmagnetized in response to the relatively high frequency whistler fluctuations, is by
216 means of the Landau resonance at $v_\perp = \omega_r/k_\perp \cong (k_{||} c/\omega_e)\, c\Omega_e/\omega_e$, so a larger simulation box
217 and longer wavelengths correspond to a smaller resonant ion velocity. This implies that
218 the resonant modes move from the tail of the perpendicular velocity distribution toward
219 the thermal part of the distribution, resonating with a larger number of ions and therefore
220 leading to stronger ion heating. *Howes* [2010] has proposed a scenario for plasma
221 heating by kinetic Alfven wave turbulence in which the maximum dissipation on the ions
222 is at wavelengths of the order of the thermal ion gyroradius; the turbulent energy which
223 remains is then carried by the forward cascade down to electron dissipation at thermal

224 electron gyroradii. Applying this scenario to magnetosonic-whistler turbulence, the
225 assumed source of the long-wavelength initial fluctuations in our simulations, the
226 increasing ion heating at larger simulation box sizes leaves successively less energy at
227 electron fluctuation scales, implying, as our simulations demonstrate, less electron
228 heating.

229 Further simulations are necessary to gain a more complete understanding of how
230 short-wavelength turbulence dissipates its energy in collisionless plasmas. It would be
231 useful to examine the relative heating of electrons and ions by whistler turbulence as
232 functions of the dimensionless parameters β_e, ε_o and T_e/T_i, particularly toward values
233 appropriate for the solar wind near 1 AU, that is, $\beta_e \cong 1$ and $\varepsilon_o << 1$. Each of these
234 parametric studies can be addressed now using available supercomputer resources. It
235 would be interesting to compare the ion/electron heating ratio as a function of the initial
236 whistler fluctuation energy density against the large-scale turbulence PIC simulation
237 results of *Wu et al.* [2013] which show an increase in this ratio with increasing initial
238 fluctuation energy.

239 However, perhaps the most important parametric study of this type concerns
240 variations in the characteristic wavelengths of the turbulence. As longer wavelength
241 fluctuations correspond to weaker electron and stronger ion heating and turbulent spectra
242 usually increase in amplitude with increasing wavelength, it is important to push 3D PIC
243 simulations to the regime of $kc/\omega_e < 0.05$. Unfortunately, this requires the calculations to
244 be carried out in successively larger simulation boxes, requiring computational resources
245 that are not available to most researchers pursuing this subject (However, see *Karimabadi*
246 *et al.,* 2013). As computing capacity continues to increase, our ability to more

247 completely address the important issue of short-wavelength turbulent dissipation will
248 similarly increase.
249
250 **Acknowledgments.** The research by R. Scott Hughes, S. Peter Gary, and Joseph
251 Wang was supported largely by the National Science Foundation (NSF) grant AGS-
252 1202603 under the NSF/DOE Partnership in Basic Plasma Science and Engineering.
253 Computational resources supporting this work were provided by the NASA High-End
254 Computing (HEC) Program through the NASA Advanced Supercomputing (NAS)
255 Division at Ames Research Center, as well as by the Yellowstone supercomputer
256 sponsored by the NSF at the Computational and Information Systems Laboratory of the
257 National Center for Atmospheric Research. The computer-generated data used to
258 produce the results described here are archived at the University of Southern California
259 and are available from Dr. Joseph Wang.
260
261 **References**
262 Bale, S. D., P. J. Kellogg, F. S. Mozer, T. S. Horbury, and H. Rème (2005), Measurement
263 of the electric fluctuation spectrum of magnetohydrodynamic turbulence, *Phys. Rev.*
264 *Lett., 94,* 215002.
265 Bourouaine, S., O. Alexandrova, E. Marsch, and M. Maksimovic (2012), On spectral
266 breaks in the power spectra of magnetic fluctuations in fast solar wind between 0.3
267 and 0.9 AU, *Ap. J., 749,* 102.
268 Chandran, B. D. G., B. Li, B. N. Rogers, E. Quataert, and K. Germaschewski (2010),
269 Perpendicular ion heating by low-frequency Alfven-wave turbulence in the solar

wind. *Ap. J., 720(1),* 503.

Chang, O., S. P. Gary, and J. Wang (2011), Whistler turbulence forward cascade: Three-dimensional particle-in-cell simulations, *Geophys. Res. Lett., 38,* L22102.

Chang, O., S. P. Gary, and J. Wang (2013), Whistler turbulence and variable electron beta: Three-dimensional particle-in-cell simulations, *J. Geophys. Res., 118,* 2824.

Chang, O., S. P. Gary, and J. Wang (2014), Energy dissipation by whistler turbulence: Three-dimensional particle-in-cell simulations, *Phys. Plasmas, 21,* 052305.

Chen, C. H. K., S. Boldyrev, Q. Xia, and J. C. Perez (2013), Nature of subproton scale turbulence in the solar wind, *Phys. Rev. Lett., 110,* 225002.

Cranmer, S. (2014), Ensemble simulations of proton heating in the solar wind via turbulence and ion cyclotron resonance, *Ap. J. Supplement Series,* in press.

Gary, S. P. (1993), Theory of space plasma microinstabilities, Cambridge University Press, New York.

Gary, S. P., and S. Saito (2003), Particle-in-cell simulations of Alfven-cyclotron wave scattering: Proton velocity distributions, *J. Geophys. Res., 108,* 1194.

Gary, S. P., S. Saito, and H. Li (2008), Cascade of whistler turbulence: Particle-in-cell simulations, *Geophys. Res. Lett., 35,* L02104.

Gary, S. P., O. Chang, and J. Wang (2012), Forward cascade of whistler turbulence: Three-dimensional particle-in-cell simulations, *Ap. J., 755,* 142.

He, J., C. Tu, E. Marsch, and S. Yao (2012), Do oblique Alfven/ion-cyclotron or fast mode/whistler waves dominate the dissipation of solar wind turbulence near the proton inertial length?, *Ap. J., 745,* L8.

292 Hellinger, P., L. Matteini, S. Štverák, P. Travnicek, and E. Marsch (2011), Heating and
293 cooling of protons in the fast solar wind between 0.3 and 1 AU: Helios revisited, *J.*
294 *Geophys. Res., 116,* A09105.
295 Hellinger, P., P. M. Travnıcek, S. Štverák, L. Matteini, and M. Velli (2013), Proton thermal
296 energetics in the solar wind: Helios reloaded, *J. Geophys. Res., 118,* 1.
297 Hollweg, J., and P. Isenberg (2002), Generation of the fast solar wind: A review with
298 emphasis on the resonant cyclotron interaction, *J. Geophys. Res., 107(A7),* 1147.
299 Howes, G. G. (2010), A prescription for the turbulent heating of astrophysical plasmas,
300 *Mon. Not. R. Astron. Soc, 409,* L104.
301 Howes, G. G., W. Dorland, S. Cowley, G. Hammett, E. Quataert, A. Schekochihin, and T.
302 Tatsuno (2008a), Kinetic simulations of magnetized turbulence in astrophysical
303 plasmas, *Phys. Rev. Lett., 100,* 065004.
304 Howes, G. G., S. C. Cowley, W. Dorland, G. W. Hammett, E. Quataert, A. A.
305 Schekochihin, and T. Tatsuno (2008b), Howes et al. reply, *Phys. Rev. Lett., 101,*
306 149502.
307 Howes, G. G., J. M. TenBarge, W. Dorland, E. Quataert, A. A. Schekochihin, R. Numata,
308 and T. Tatsuno (2011), Gyrokinetic simulations of solar wind turbulence from ion to
309 electron scales, *Phys. Rev. Lett., 107,* 035004.
310 Karimabadi, H., V. Roytershteyn, M. Wan, W. H. Matthaeus, W. Daughton, P. Wu, M.
311 Shay, B. Loring, J. Borovsky, E. Leonardis, S. C. Chapman, and T. K. M. Nakamura
312 (2013), Coherent structures, intermittent turbulence, and dissipation in high-
313 temperature plasmas, *Phys. Plas, 20,* 012303.

314 Kiyani, K. H., S. C. Chapman, F. Sahraoui, B. Hnat, O. Fauvarque, and Yu. V.
315 Khotyaintsev (2013), Enhanced magnetic compressibility and isotropic scale-
316 invariance at sub-ion Larmor scales in solar wind turbulence, *Ap. J., 763,* 10.
317 Leamon, R. J., C. W. Smith, N. F. Ness, W. H. Matthaeus, and H. K. Wong (1998),
318 Observational constraints on the dynamics of the interplanetary magnetic field
319 dissipation range, *J. Geophys. Res., 103,* 4775.
320 Markovskii, S. A., B. J. Vasquez, and C. W. Smith (2008), Statistical analysis of the high-
321 frequency spectral break of the solar wind turbulence at 1 AU, *Ap. J., 675,* 1576.
322 Matthaeus, W. H., S. Servidio, and P. Dmitruk (2008), Comment on "Kinetic simulations
323 of magnetized turbulence in astrophysical plasmas," *Phys. Rev. Lett., 101,* 149501.
324 Narita, Y., S. P. Gary, S. Saito, K.-H. Glassmeier, and U. Motschmann (2011), Dispersion
325 relation analysis of solar wind turbulence, *Geophys. Res. Lett., 38,* L05101.
326 Perschke, C., Y. Narita, S. P. Gary, U. Motschmann, and K.-H. Glassmeier (2013),
327 Dispersion relation analysis of turbulent magnetic field fluctuations in fast solar
328 wind, *Ann. Geophys., 31,* 1949.
329 Perschke, C., Y. Narita, U. Motschmann, and K.-H. Glassmeier (2014), Multi-spacecraft
330 observations of linear modes and sideband waves in ion-scale solar wind turbulence,
331 *Ap. J. Lett., 793,* L25.
332 Podesta, J. J., J. E. Borovsky, and S. P. Gary (2010), A kinetic Alfven wave cascade
333 subject to collisionless damping cannot reach electron scales in the solar wind at 1
334 AU, *Ap. J., 712*, 685.

335 Sahraoui, F., M L. Goldstein, P. Robert, and Yu. V. Khotyaintsev (2009), Evidence of a
336 cascade and dissipation of solar-wind turbulence at the electron gyroscale, *Phys.*
337 *Rev. Lett., 102,* 231102.
338 Sahraoui, F., M L. Goldstein, G. Belmont, P. Canu, and L. Rezeau (2010), Three
339 dimensional anisotropic *k* spectra of turbulence at subproton scales in the solar wind,
340 *Phys. Rev. Lett., 105,* 131101.
341 Sahraoui, F., S. Y. Huang, G. Belmont, M. L. Goldstein, A. Retino, P. Robert, and J.
342 DePatoul (2013), Scaling of the electron dissipation range of solar wind turbulence,
343 *Ap. J., 777,* 15.
344 Saito, S., and S. P. Gary (2012), Beta dependence of electron heating in decaying whistler
345 turbulence: Particle-in-cell simulations, *Phys. Plasmas, 19,* 012312.
346 Saito, S., and Y. Nariyuki (2014), Perpendicular ion acceleration in whistler turbulence,
347 *Phys. Plasmas, 21,* 042303.
348 Saito, S., S. P. Gary, H. Ki, and Y. Narita (2008), Whistler turbulence: Particle-in-cell
349 simulations, *Phys. Plasmas, 15,* 102305.
350 Saito, S., S. P. Gary, and Y. Narita (2010), Wavenumber spectrum of whistler turbulence:
351 Particle-in-cell simulation, *Phys. Plasmas, 17,* 122316.
352 Salem, C. S., G. G. Howes, D. Sundkvist, S. D. Bale, C. C. Chaston, C. H. K. Chen, and F.
353 S. Mozer (2012), Identification of kinetic Alfven wave turbulence in the solar wind,
354 *Ap. J., 745,* L9.
355 Smith, C. W., B. J. Vasquez, and J. V. Hollweg (2012), Observational constraints on the
356 role of cyclotron damping and kinetic Alfven waves in the solar wind, *Ap. J., 745,* 8.

357 Svidzinski, V. A., H. Li, H. A. Rose, B. J. Albright, and K. J. Bowers (2009), Particle in
358 cell simulations of fast magnetosonic wave turbulence in the ion cyclotron frequency
359 range, *Phys. Plasmas, 16,* 122310.
360 TenBarge, J., and G. G. Howes (2013), Current sheets and collisionless damping in kinetic
361 plasma turbulence, *Ap. J., 771,* L27.
362 TenBarge, J. M., G. G. Howes, and W. Dorland (2013), Collisionless damping at electron
363 scales in solar wind turbulence, *Ap. J., 774,* 139.
364 Villasenor, J., and O. Buneman (1992), Rigorous charge conservation for local
365 electromagnetic field solvers, *Comput. Phys. Commun.,69,* 306.
366 Wang, J., P. Liewer, and V. Decyk (1995), 3D electromagnetic plasma particle simulations
367 on a MIMD parallel computer, *Comput. Phys. Commun., 69,* 306.
368 Wu, P., M. Wan, W. Matthaeus, M. Shay, and M. Swisdak (2013), von Karman energy
369 decay and heating of protons and electrons in a kinetic turbulent plasma. *Phys. Rev.*
370 *Lett., 111(12),* 121105.
371 Xia, Q., J. C. Perez, B. D. Chandran, and E. Quataert (2013), Perpendicular ion heating by
372 reduced magnetohydrodynamic turbulence, *Ap. J., 776,* 90.